Journal of Fluids and Structures 77 (2018) 196–212

Contents lists available at ScienceDirect

Journal of Fluids and Structures

journal homepage: www.elsevier.com/locate/jfs

A numerical investigation on piezoelectric energy harvesting from Vortex-Induced Vibrations with one and two degrees of freedom

Guilherme R. Franzini *, Lucas O. Bunzel

Offshore Mechanics Laboratory, Escola Politécnica, University of São Paulo, Brazil

HIGHLIGHTS

- Energy harvesting from 1-dof and 2-dof VIV.
- Mathematical models for systems.
- In-line oscillations increase the energy harvesting efficiency.

ARTICLE INFO

Article history:
Received 19 July 2017
Received in revised form 2 December 2017
Accepted 4 December 2017
Available online 29 December 2017

Keywords:
Energy harvesting
Vortex-Induced Vibrations
Piezoelectric effects
Numerical investigation
Wake-oscillator models

ABSTRACT

This paper presents numerical investigations into the dynamics of a rigid cylinder, mounted on elastic supports fitted with piezoelectric harvesters and subjected to the Vortex-Induced Vibrations (VIV) phenomenon. Hydrodynamic loads are considered by wake-oscillators models, whereas linear constitutive equations are adopted aiming at coupling the solid and electric oscillators. The main objective is to highlight the influence of an additional structural degree of freedom (namely, in-line oscillations) on the dynamics of the fluid–solid-electric system.

For a particular set of dimensionless parameters that define the harvester circuits, oscillation amplitudes, electric tension and harvested power are obtained for different reduced velocities. Among other findings, the simultaneous presence of in-line and cross-wise oscillations can be emphasized to lead to a marked increase in the maximum energy harvesting efficiency.

In addition to this analysis, a sensitivity study with respect to the influence of the dimensionless quantities that characterize the piezoelectric harvesters is carried out. The study shows that the energy harvesting efficiency can be increased by up to 50% for a particular reduced velocity.

1. Introduction

Flow-induced vibrations phenomena (FIV) cover a comprehensive class of generally non-linear problems that lead to self-excited oscillations. Examples of FIV phenomena include galloping, flutter and vortex-induced vibrations (VIV), the latter being the focus of this contribution. The textbooks written by Blevins (2001), Naudascher and Rockwell (2005) and Païdoussis and de Langre (2011) are examples of surveys on this topic.

* Corresponding author.
E-mail address: gfranzini@usp.br (G.R. Franzini).

https://doi.org/10.1016/j.jfluidstructs.2017.12.007
0889-9746/

Nomenclature

$\omega_{n,y}$ and $\omega_{n,x}$ Cylinder's natural frequencies
m_s, m_f and m_d Structural mass, potential added mass and mass of fluid displaced by the cylinder
U_∞ Free-stream velocity
ω_f Vortex-shedding frequency
D, L Cylinder diameter and length
ρ Fluid density
k_y and k_x Spring stiffnesses
c_y and c_x Damping constants
R_y and R_x Electric resistances
$C_{P,y}$ and $C_{P,x}$ Capacitances
θ_y and θ_x Electro-mechanical coupling constants
t Dimensional time
Y and X Dimensional displacements
V_y and V_x Dimensional electric tensions
V_0 Reference electric tension
q_y and q_x Wake variables
τ Dimensionless time
y and x Dimensionless displacements
v_y and v_x Dimensionless electric tensions
ϵ_y, A_y, ϵ_x and A_x Parameters of the wake-oscillator models
m^* and C_a Mass parameter and potential added mass coefficient
ζ_y and ζ_x structural damping ratios
U_r Reduced velocity
St Strouhal number
$C_{y,v}$, $C_{x,v}$, $C_{L,v}$ and $C_{D,v}$ Force coefficients due to vortex-shedding
$\hat{C}_L^0$ and $\hat{C}_D^0$ Amplitude of the lift and drag coefficients observed for a stationary cylinder
$\overline{C}_D^0$ Mean drag coefficient observed for a stationary cylinder
$\sigma_{1,y}$, $\sigma_{1,x}$, $\sigma_{2,y}$ and $\sigma_{2,x}$ Dimensionless quantities related to the piezoelectric harvesters
$\eta_{el,y}$ and $\eta_{el,x}$ Dimensionless electric power harvested at cross-wise and in-line harvesters

VIV is a very interesting fluid–structure interaction problem commonly found in several engineering applications. Its self-excited and self-limited character has attracted attention from both the industrial and the academic communities in the last decades. Fundamental aspects of flow around cylinders can be found, for example, in the reviews by Bearman (1984, 2011), Parkinson (1989), Williamson and Govardhan (2004), Sarpkaya (1979, 2004). Besides these reviews, a series of investigations have focused on different aspects of the phenomenon has been published since the 1970s. Examples of studies include those related to the cylinder response to oscillatory flows (Sarpkaya, 1977, 1986; Sumer and Fredsøe, 1988), the wake patterns (Williamson and Roshko, 1988; Williamson, 1996), reduced-order modeling approaches (Hartlen and Currie, 1970; Iwan and Blevins, 1974; Skop and Griffin, 1975; Skop and Balasubramanian, 1997) and the dynamics of flexible cylinders (Lyons and Patel, 1986; Hover et al., 1997; Pesce and Fujarra, 2000; Fujarra et al., 2001; Chaplin et al., 2005b, a; Huera-Huarte and Bearman, 2009a, b).

Even though the aspects aforementioned are important, we focus on the fundamental problem of a rigid cylinder mounted on an elastic support free to oscillate only in the cross-wise direction (direction orthogonal to the free-stream velocity). For this condition (herein named 1-dof VIV), it is well known that relevant oscillations (with maximum amplitude close to one diameter D) are observed in the range of reduced velocities $3 < U_r = U_\infty/f_{n,y}D < 12$, being U_∞ the free-stream velocity and $f_{n,y}$ the natural frequency obtained with the cylinder submerged in a still fluid. In this range of reduced velocities, the vortex-shedding frequency f_f is close to $f_{n,y}$ and the lock-in phenomenon is observed.

Experimental results presented in Khalak and Williamson (1999) revealed the existence of distinct response branches depending on the mass-damping parameter $m^*\zeta_y$, where m^* is the mass parameter, defined as the ratio between the oscillating mass and the mass of fluid displaced by the cylinder and ζ_y is the damping ratio. The latter reference also discussed the dependence of the hydrodynamic force coefficients as functions of U_r, as well as distinct vortex-shedding pattern.

Since the early 2000s, focus has also lain on the problem of a rigid cylinder free to oscillate in both in-line (parallel to the free-stream velocity) and cross-wise directions, referred to throughout this paper as 2-dof VIV. As verified, for example, in Jauvtis and Williamson (2004), Stappenbelt and Lalji (2008), Blevins and Coughran (2009), Freire and Meneghini (2010) and Franzini et al. (2012) there are marked differences between 1-dof and 2-dof VIV. Among these differences, we can highlight the dependence of in-line oscillations magnitude with $m^*\zeta$, the increase in cross-wise response due to in-line oscillations and a new vortex-shedding pattern.

Due to its intrinsic complex character, VIV is commonly investigated using both experimental and computational approaches. Computational studies on VIV can be carried out using high-order hierarchical models such as those based on the Finite Volume Method or using reduced-order models. In the latter approach, the wake behavior is modeled using a nonlinear oscillator coupled to a structural one. The approach is also named as wake-oscillator model and has been used in the last four decades in a series of studies for both 1-dof (Iwan and Blevins, 1974; Facchinetti and de Langre, 2004; Gabbai and Benaroya, 2005, 2008; Ogink and Metrikine, 2010) and 2-dof VIV (Furnes and Sørensen, 2007; Srinil and Zanganeh, 2012; Dhanwani et al., 2013; Zanganeh and Srinil, 2014).

Recently, investigations aimed to convert part of structural kinetic energy into another kind of energy, such as, electric or gravitational energy. Focusing on obtaining electric energy from structural oscillations, we can highlight two conversion mechanisms based on electromagnetic or piezoelectric effects. A comprehensive review regarding piezoelectric energy harvesting can be found in the textbook by Erturk and Inman (2011).

Particularly, energy harvesting from flow-induced vibrations phenomena is an interesting approach, since most FIV problems lead to self-excited oscillations. A series of investigations focuses on energy harvesting from both galloping and flutter phenomena. A review of energy harvesting from flapping foils can be found in Xiao and Zhu (2014).

Tang and Païdoussis (2009) proposed the concept of the flutter-mill, in which a cantilevered flexible plate embedded with a conductor oscillates between two magnetic plates. Barrero-Gil et al. (2010) focused on energy harvesting from transverse galloping of a prism, investigating the effects of the cross-section geometry on the harvested energy at the dashpot. Energy harvesting from flexible plates or flags in fluttering is also investigated by Doaré and Michelin (2011), which presented a linear stability analysis of a piezoelectric plate subjected to axial flow. Fernandes and Armandei (2014) experimentally investigated how the torsional galloping of a rigid and pivoted plate can be used to lift weights. For plates with 0.2 m and 0.3 m in chord length and 0.45 m in depth tested on a towing tank facility, the authors showed to be possible to lift a mass of 0.227 kg at a 2.2 m height. Numerical studies presented in Franzini et al. (2016) and in Franzini et al. (2017) showed that parametric excitation can significantly affect piezoelectric energy harvesting from a square prism. Wind tunnel experiments with prisms coupled to magnets and subjected to galloping were detailed in Hémon et al. (2017). As an example of result, the authors plotted the harvested electrical power as a function of the load resistance, obtaining a maximum value close to 0.5 mW. In their results, the authors pointed out that despite the low efficiency of this energy harvester, it can be improved and applied to situations in which standard turbines cannot be used.

A series of efforts into energy harvesting from VIV phenomenon is also found. Bernitsas et al. (2006) presents the concept of VIVACE (Vortex-Induced Vibration Aquatic Clean Energy), a device based on a series of cylinders in tandem arrangement that uses the electromagnetic effect to convert structural kinetic energy into electricity. In Mehmood et al. (2013), the authors investigated piezoelectric energy harvesting using the Computational Fluids Dynamics (CFD) approach to model the fluid forces on the cylinder, showing that the electric resistance plays an important role at the onset of synchronization.

Numerical studies on energy harvesting from VIV can also be found in Grouthier et al. (2012, 2014). In these papers, fluid forces were modeled using the wake-oscillator concept and energy harvested at dashpots were obtained. Among other findings, the authors pointed out a peak of energy harvesting efficiency close to 0.23 for 1-dof VIV, as well as the possibility of high-efficiency regions for flexible cylinders. Energy harvesting from flexible cylinder VIV was also investigated by Antoine et al. (2016b), which showed the loss of efficiency on flexible structures to be less sensitive than rigid cylinder elastically supported to flow fluctuations around the value corresponding to the maximum energy harvesting efficiency. Antoine et al. (2016a) employed adjoint methods in order to optimize the distribution of harvesters along a straight cable subjected to VIV. As a major conclusion, the authors recommend to distribute the harvesters close to one of the attachments points.

Arionfard and Nishi (2017) experimentally studied energy harvesting from a pivoted rigid cylinder subjected to VIV. A sensitivity study regarding the energy harvesting efficiency as functions of different parameters of the set-up was carried out, allowing obtaining a maximum harvested power close to 60 mW. Another conclusion drawn by the authors is that the increase in the Reynolds number does not necessarily increase the energy harvesting efficiency.

Nishi et al. (2017) also presented an experimental investigation on electro-magnetic energy harvesting from VIV. In this latter paper, the authors inserted a secondary cylinder between a cylinder excited by VIV and the generator. This secondary cylinder allowed enhancing the range of free-stream velocities in which the energy harvesting is effective. Experimental results indicated that the electric tension can reach 9 V. The recent paper written by Soti et al. (2017) numerically studied the dynamics of a system composed of a cylinder fixed to a magnet that can move in the direction of a coil. An interesting result pointed out by the authors is a value of maximum dimensionless harvested power equal to 0.13.

Piezoelectric energy harvesting from VIV has also been focused by recent investigations. Akaydin et al. (2012) carried out a series of experiments in a wind tunnel facility with a rigid cylinder assembled to a flexible beam fitted with a piezoelectric layer. Among other findings, the authors showed that the harvested electric power experimentally obtained is close to 0.1 mW. A similar problem was also analytically studied by Dai et al. (2014), which also included the effects of base excitation.

Zhang et al. (2017) also investigated energy harvesting from VIV in a wind tunnel. In their paper, the rigid cylinder was assembled to a flexible piezoelectric beam and the presence of two magnets led to nonlinear restoring forces. The authors showed that the mentioned nonlinearity increased the harvested electric power by up to 29%. Bunzel and Franzini (2017) numerically studied energy harvesting from 2-dof VIV using a wake-oscillator model. The authors showed curves of oscillation amplitudes and energy harvesting efficiency as functions of the reduced velocity and for different piezoelectric dimensionless quantities.

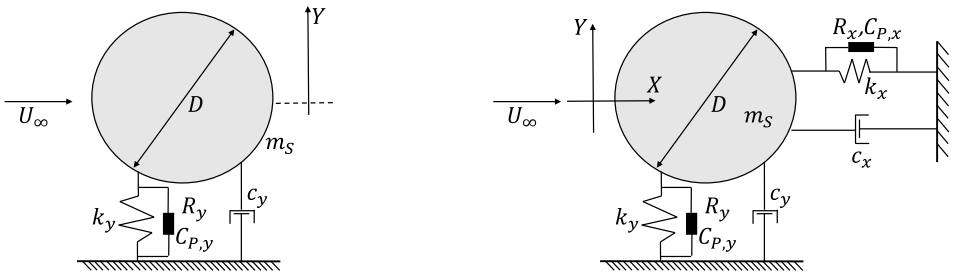

(a) 1-dof VIV with a piezoelectric harvester.

(b) 2-dof VIV with two piezoelectric harvesters.

Fig. 1. Schematic representation of the problems.

This literature review shows that piezoelectric energy harvesting from 2-dof VIV is not commonly investigated. We here aim to contribute to the context of energy harvesting from VIV, enhancing the discussions presented in Bunzel and Franzini (2017). The focus lies on rigid cylinders mounted on elastic supports fitted with piezoelectric harvesters. Fluid forces are modeled by wake-oscillator models for both 1-dof and 2-dof VIV. The main contribution of this paper is to illustrate the differences caused by the presence of simultaneous in-line and cross-wise oscillations. In addition, we present a sensitivity study regarding the influence of two dimensionless quantities that define the piezoelectric circuits in the harvested electric power for a particular reduced velocity.

This paper is structured in five Sections. After this literature review, Section 2 is dedicated to the derivation of the mathematical model. Section 3 discusses the analysis methodology. Section 4 presents and discusses the numerical results. Finally, the final remarks are presented in Section 5.

2. Mathematical models

This Section presents the mathematical model for the problems investigated herein and sketched in Fig. 1. For both problems, the rigid cylinder has total mass m_s, length L and is immersed in a fluid of density ρ. For the 1-dof VIV (Fig. 1(a)), the cylinder is assembled to an elastic base with linear stiffness and damping (k_y and c_y respectively). For this condition, the piezoelectric harvester is defined by its resistance R_y, capacitance $C_{P,y}$ and electro-mechanical coupling term θ_y.

For 2-dof VIV (see Fig. 1(b)), the cylinder is mounted on a support with linear cross-wise stiffness and damping constants equal to k_y and c_y respectively. In the in-line direction, the elastic support has stiffness and damping equal to k_x and c_x, respectively. Both in-line and cross-wise directions present independent piezoelectric harvesters, so that the electric power can be harvested from to the motion in both directions. The cross-wise piezoelectric harvester has resistance R_y, capacitance $C_{P,y}$ and electro-mechanical coupling term θ_y, while these properties are R_x, $C_{P,x}$ and θ_x for the in-line harvester.

For the sake of organization, the wake-oscillator models for 1-dof and 2-dof (properly adopted in order to take into account the piezoelectric effect), will be presented in Sections 2.1 and 2.2 respectively.

2.1. Mathematical model: 1-dof VIV

The fluid forces on the cylinder follow the methodology presented in Facchinetti and de Langre (2004) and modified by Ogink and Metrikine (2010) a few years later. The van der Pol's equation is commonly adopted aiming at representing the fluid dynamics. Following the suggestion by Facchinetti and de Langre (2004), an acceleration coupling scheme is used for the solid–fluid interaction. Finally, a constitutive equation couples the solid-electric oscillators, similarly to what was carried out in Mehmood et al. (2013). The solid–fluid-electric system is governed by Eqs. (1)–(3).

$$(m_s + m_f)\frac{d^2Y}{dt^2} + c_y\frac{dY}{dt} + k_yY - \theta_yV_y = \frac{1}{2}\rho U_\infty^2 DLC_{y,v} \tag{1}$$

$$\frac{d^2q_y}{dt^2} + \epsilon_y\omega_f(q_y^2 - 1)\frac{dq_y}{dt} + \omega_f^2 q_y = \frac{A_y}{D}\frac{d^2Y}{dt^2} \tag{2}$$

$$C_{P,y}\frac{dV_y}{dt} + \frac{V_y}{R_y} + \theta_y\frac{dY}{dt} = 0 \tag{3}$$

The wake of a stationary cylinder is commonly described by Eq. (2), but taking its right-hand side as null. This condition leads to a limit-cycle periodic solution with amplitude $\hat{q}_y = 2$ and frequency equal to the vortex-shedding frequency $\omega_f = 2\pi StU_\infty/D$, being St the Strouhal number. Considering that the natural frequency in still water is given by $\omega_{n,y} =$

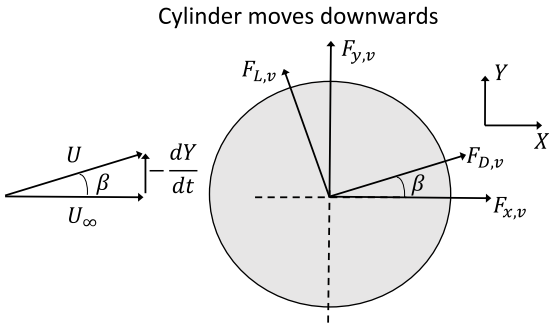

Fig. 2. Sketch of the fluid loads acting on the cylinder. 1-dof VIV.

$2\pi f_{n,y} = \sqrt{k_y/(m_s + m_f)}$, a series of dimensionless quantities can be defined as:

$$\zeta_y = \frac{c_y}{2(m_s + m_f)\omega_{n,y}}, U_r = \frac{U_\infty}{f_{n,y}D}, St = \frac{\omega_f D}{2\pi U_\infty}, \quad y = \frac{Y}{D}, \quad \tau = \omega_{n,y}t, \quad v_y = \frac{V_y}{V_0}$$

$$m^* = \frac{m_s}{m_d}, \quad C_a = \frac{m_f}{m_d}, \quad \sigma_{2,y} = \frac{1}{C_{P,y}R_y\omega_{n,y}}, \quad \sigma_{1,y} = \frac{\theta_y^2}{C_{P,y}(m_s + m_f)\omega_{n,y}^2}$$

being $V_0 = \frac{(m_s+m_f)\omega_{n,y}^2 D}{\theta_y}$ a reference electric tension and $m_d = \rho\pi D^2 L/4$ the mass of fluid displaced by the cylinder. Defining $(\dot{})$ as the derivative with respect to dimensionless time τ, Eqs. (1)–(3) are rewritten as:

$$\ddot{y} + 2\zeta_y\dot{y} + y - v_y = \frac{1}{2\pi^3}\frac{U_r^2}{(m^* + C_a)}C_{y,v} \tag{4}$$

$$\ddot{q}_y + \epsilon StU_r(q_y^2 - 1)\dot{q}_y + (StU_r)^2 q_y = A_y\ddot{y} \tag{5}$$

$$\dot{v}_y + \sigma_{2,y}v_y + \sigma_{1,y}\dot{y} = 0 \tag{6}$$

Now, we focus on describing the relation between $C_{y,v}$ and wake variable q_y. Fig. 2 presents a schematic representation of the cylinder oscillating in the fluid and clearly reveals the geometric relations given by Eqs. (7)–(9).

$$U = \sqrt{U_\infty^2 + \left(\frac{dY}{dt}\right)^2} = U_\infty\sqrt{1 + \left(\frac{2\pi\dot{y}}{U_r}\right)^2} \tag{7}$$

$$\sin\beta = \frac{-\frac{dY}{dt}}{U} = -\frac{2\pi\dot{y}}{U_r\sqrt{1 + \left(\frac{2\pi\dot{y}}{U_r}\right)^2}} \tag{8}$$

$$\cos\beta = \frac{U_\infty}{U} = \frac{1}{\sqrt{1 + \left(\frac{2\pi\dot{y}}{U_r}\right)^2}} \tag{9}$$

The fluid forces associated to vortex-shedding are written through Eqs. (10)–(12).

$$F_{D,v} = \frac{1}{2}\rho U^2 DLC_{D,v} \tag{10}$$

$$F_{L,v} = \frac{1}{2}\rho U^2 DLC_{L,v} \tag{11}$$

$$F_{y,v} = \frac{1}{2}\rho U_\infty^2 DLC_{y,v} = F_{L,v}\cos\beta + F_{D,v}\sin\beta \tag{12}$$

Hence, the cross-wise force coefficient is given by:

$$C_{y,v} = \left(\frac{U}{U_\infty}\right)^2 (C_{L,v}\cos\beta + C_{D,v}\sin\beta) = \left(C_{L,v} - \frac{C_{D,v}2\pi\dot{y}}{U_r}\right)\sqrt{1 + \left(\frac{2\pi\dot{y}}{U_r}\right)^2} \tag{13}$$

where $C_{L,v}$ e $C_{D,v}$ are the force coefficients observed in the flow around a stationary cylinder (Ogink and Metrikine, 2010). Moreover, the oscillatory lift coefficient is related to wake variable q_y in Eq. (14).

$$C_{L,v} = \frac{q_y}{\hat{q}_y}\hat{C}_L^0 \tag{14}$$

where $\hat{C}_L^0$ is the amplitude of the lift coefficient observed in stationary cylinder. Eq. (14) can be substituted into Eq. (4) leading to the following system of differential equations:

$$\ddot{y} + 2\zeta_y\dot{y} + y - v_y = \frac{1}{2\pi^3}\frac{U_r^2}{(m^* + C_a)}\left[\left(\frac{q_y}{\hat{q}_y}\hat{C}_L^0 - \frac{C_{D,v}2\pi\dot{y}}{U_r}\right)\sqrt{1 + \left(\frac{2\pi\dot{y}}{U_r}\right)^2}\right] \tag{15}$$

$$\ddot{q}_y + \epsilon StU_r(q_y^2 - 1)\dot{q}_y + (StU_r)^2 q_y = A_y\ddot{y} \tag{16}$$

$$\dot{v}_y + \sigma_{2,y}v_y + \sigma_{1,y}\dot{y} = 0 \tag{17}$$

Note that Eqs. (15) and (16) represent the dynamics of the cylinder subjected to 1-dof VIV if $\sigma_{1,y} = \sigma_{2,y} = v_y(0) = 0$ (pure 1-dof VIV). These equations are the same obtained by Ogink and Metrikine (2010) in their wake-oscillator model but re-written using a different dimensionless time τ.

For energy harvesting, the electric power ($P_{el,y}$) should be computed, expressed in the dimensional form as:

$$P_{el,y} = \frac{V_y^2}{R_y} \tag{18}$$

This power is made dimensionless with respect to the flux of fluid kinetic energy across the cylinder front area. Using this concept and the quantities already defined, one can obtain:

$$\eta_{el,y} = \frac{P_{el,y}}{1/2\rho U_\infty^3 DL} = \frac{4\pi^4}{U_r^3}\frac{\sigma_{2,y}}{\sigma_{1,y}}(m^* + C_a)v_y^2 \tag{19}$$

Observe that $\eta_{el,y}$ can be interpreted as the energy harvesting efficiency, similarly to what was discussed by Grouthier et al. (2014). Their paper, however, discussed energy harvesting by means of the power dissipated at the dashpot.

2.2. Mathematical model: 2-dof VIV

This Subsection presents the derivation of the mathematical model corresponding to a rigid cylinder free to oscillate both in the cross-wise and in the in-line directions. Similarly to what was carried out in Section 2.1 for the 1-dof VIV case and by Srinil and Zanganeh (2012) and (Dhanwani et al., 2013) for 2-dof VIV, van der Pol's equations are used for modeling the fluid forces. As already mentioned, we consider that there are piezoelectric circuits that allow energy harvesting from oscillations in both directions independently. Hence, the solid–fluid-electric system is governed by Eqs. (20)–(25).

$$(m_s + m_f)\frac{d^2Y}{dt^2} + c_y\frac{dY}{dt} + k_yY - \theta_yV_y = \frac{1}{2}\rho U_\infty^2 DLC_{y,v} \tag{20}$$

$$\frac{d^2q_y}{dt^2} + \epsilon_y\omega_f(q_y^2 - 1)\frac{dq_y}{dt} + \omega_f^2 q_y = \frac{A_y}{D}\frac{d^2Y}{dt^2} \tag{21}$$

$$(m_s + m_f)\frac{d^2X}{dt^2} + c_x\frac{dX}{dt} + k_xX - \theta_xV_x = \frac{1}{2}\rho U_\infty^2 DLC_{x,v} \tag{22}$$

$$\frac{d^2q_x}{dt^2} + \epsilon_x\omega_f(q_x^2 - 1)\frac{dq_x}{dt} + (2\omega_f)^2 q_x = \frac{A_x}{D}\frac{d^2X}{dt^2} \tag{23}$$

$$C_{P,y}\frac{dV_y}{dt} + \frac{V_y}{R_y} + \theta_y\frac{dY}{dt} = 0 \tag{24}$$

$$C_{P,x}\frac{dV_x}{dt} + \frac{V_x}{R_x} + \theta_x\frac{dX}{dt} = 0 \tag{25}$$

For the 2-dof VIV problem, both dimensionless time τ and reduced velocity U_r are defined as discussed in the previous Subsection. In addition to the quantities already defined for the 1-dof VIV problem, consider the following parameters:

$$\omega_{n,x} = \sqrt{\frac{k_x}{m_s + m_f}},\ \zeta_x = \frac{c_x}{2(m_s + m_f)\omega_{n,x}},\ x = \frac{X}{D},\quad v_x = \frac{V_x}{V_0}$$

$$\sigma_{2,x} = \frac{1}{C_{P,x}R_x\omega_{n,x}},\quad \sigma_{1,x} = \frac{\theta_x^2}{C_{P,x}(m_s + m_f)\omega_{n,x}^2},\quad f^* = \frac{\omega_{n,x}}{\omega_{n,y}},\quad \theta^* = \frac{\theta_x}{\theta_y}$$

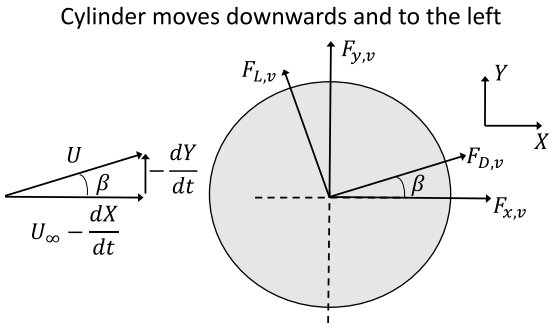

Fig. 3. Sketch of the fluid loads acting on the cylinder. 2-dof VIV.

In the 2-dof VIV problem, the fluid forces acting on the cylinder are sketched in Fig. 3. From this sketch, one can easily obtain the following relations.

$$U = \sqrt{\left(U_\infty - \frac{dX}{dt}\right)^2 + \left(\frac{dY}{dt}\right)^2} = U_\infty \sqrt{1 - \frac{4\pi}{U_r}\dot{x} + \left(\frac{2\pi}{U_r}\right)^2 (\dot{x}^2 + \dot{y}^2)} \tag{26}$$

$$\sin\beta = \frac{-\frac{dY}{dt}}{U} = -\frac{2\pi\dot{y}}{U_r\sqrt{1 - \frac{4\pi}{U_r}\dot{x} + \left(\frac{2\pi}{U_r}\right)^2 (\dot{x}^2 + \dot{y}^2)}} \tag{27}$$

$$\cos\beta = \frac{U_\infty - \frac{dX}{dt}}{U} = \frac{1 - \frac{2\pi}{U_r}\dot{x}}{\sqrt{1 - \frac{4\pi}{U_r}\dot{x} + \left(\frac{2\pi}{U_r}\right)^2 (\dot{x}^2 + \dot{y}^2)}} \tag{28}$$

The hydrodynamic loads sketched in Fig. 3 are given by Eqs. (29)–(32):

$$F_{D,v} = \frac{1}{2}\rho U^2 D L C_{D,v} \tag{29}$$

$$F_{L,v} = \frac{1}{2}\rho U^2 D L C_{L,v} \tag{30}$$

$$F_{y,v} = \frac{1}{2}\rho U_\infty^2 D L C_{y,v} = F_{L,v}\cos\beta + F_{D,v}\sin\beta \tag{31}$$

$$F_{x,v} = \frac{1}{2}\rho U_\infty^2 D L C_{x,v} = -F_{L,v}\sin\beta + F_{D,v}\cos\beta \tag{32}$$

The force coefficients in the cross-wise and in the in-line directions are given in terms of the lift and drag coefficients and angle β as:

$$C_{y,v} = \left(\frac{U}{U_\infty}\right)^2 (C_{D,v}\sin\beta + C_{L,v}\cos\beta) \tag{33}$$

$$C_{x,v} = \left(\frac{U}{U_\infty}\right)^2 (C_{D,v}\cos\beta - C_{L,v}\sin\beta) \tag{34}$$

Contrary to Srinil and Zanganeh (2012) and Dhanwani et al. (2013), which considered small angles of attack β such as $\sin\beta \approx \beta$, we here kept these nonlinearities in the mathematical model. Drag and lift coefficients ($C_{D,v}$ and $C_{L,v}$ respectively) are written in terms of wake variables q_x and q_y by Eqs. (35) and (36).

$$C_{D,v} = \overline{C}_D^0 + C_D^{osc} = \overline{C}_D^0 + \frac{q_x}{\hat{q}_x}\hat{C}_D^0 \tag{35}$$

$$C_{L,v} = \frac{q_y}{\hat{q}_y}\hat{C}_L^0 \tag{36}$$

being $\overline{C}_D^0$ and $\hat{C}_D^0$ the mean value and the oscillation amplitude of the drag coefficient observed in the problem of a stationary cylinder. Substituting Eqs. (33)–(36) into Eqs. (20)–(25) and considering the dimensionless quantities already presented, the

Table 1
Properties of the experimental investigation presented in Franzini et al. (2012). Pure VIV tests.

Parameter	Value
m^*	2.6
L/D	15
$\zeta_y = \zeta_x$	7×10^{-4}
D	44.45 mm
$f_{n,y} = f_{n,x}$	0.62 Hz

solid–fluid-electric system is described by the following dimensionless equations.

$$\ddot{y} + 2\zeta_y\dot{y} + y - v_y = \frac{1}{2\pi^3}\frac{U_r^2}{(m^* + C_a)}C_{y,v} \tag{37}$$

$$\ddot{q}_y + \epsilon_y StU_r(q_y^2 - 1)\dot{q}_y + (StU_r)^2 q_y = A_y\ddot{y} \tag{38}$$

$$\ddot{x} + 2\zeta_x f^*\dot{x} + (f^*)^2 x - \theta^* v_x = \frac{1}{2\pi^3}\frac{U_r^2}{(m^* + C_a)}C_{x,v} \tag{39}$$

$$\ddot{q}_x + \epsilon_x StU_r(q_x^2 - 1)\dot{q}_x + (2StU_r)^2 q_x = A_x\ddot{x} \tag{40}$$

$$\dot{v}_y + \sigma_{2,y}v_y + \sigma_{1,y}\dot{y} = 0 \tag{41}$$

$$\dot{v}_x + f^*\sigma_{2,x}v_x + \frac{\sigma_{1,x}}{\theta^*}(f^*)^2\dot{x} = 0 \tag{42}$$

The harvested electric power obtained at the cross-wise direction piezoelectric circuit is given by Eq. (18), whereas this quantity obtained from the in-line direction is given by Eq. (43).

$$P_{el,x} = \frac{V_x^2}{R_x} \tag{43}$$

Similarly to the 1-dof VIV, electric power is made dimensionless by using the flux of kinetic energy across the cylinder front area, giving rise to the in-line energy harvesting efficiency $\eta_{el,x}$. For the 2-dof VIV case, $\eta_{el,y}$ is calculated using the same expression obtained for the 1-dof VIV case (see Eq. (19)). The in-line energy harvesting efficiency reads:

$$\eta_{el,x} = \frac{4\pi^4}{U_r^3}\frac{(\theta^*)^2}{f^*}\frac{\sigma_{2,x}}{\sigma_{1,x}}(m^* + C_a)v_x^2 \tag{44}$$

3. Analysis methodology

Eqs. (15)–(17) (1-dof VIV) and Eqs. (37)–(42) (2-dof VIV) are numerically integrated using MATLAB® ode45 function (Runge–Kutta scheme). The adopted time-step is $\Delta\tau = 0.01$ and the maximum dimensionless time is defined as $\tau_{max} = 800$. For both 1-dof and 2-dof VIV simulations, the only non-trivial initial condition is $q_y(0) = 0.01$. For avoiding the effects of transitory responses, steady-state responses are considered only for $\tau > \tau_{max}/2$. Similarly to (Franzini et al., 2013), characteristic oscillation amplitudes in the cross-wise and in the in-line directions ($\hat{y}$ and $\hat{x}$ respectively) are computed by taking the averaged value of the 10% highest *extrema* of the corresponding steady-state time-histories.

The parameters of the elastic support and the piezoelectric harvesters are assumed to be identical in the cross-wise and in the in-line directions, such that $\sigma_{1,y} = \sigma_{1,x} = \sigma_1$, $\sigma_{2,y} = \sigma_{2,x} = \sigma_2$ and $f^* = 1$. Notice, however, that the mathematical models allow a more comprehensive investigation.

As already mentioned, this investigation aims to investigate the dynamics of a cylinder coupled to piezoelectric harvesters subjected to VIV. In a first set of simulations, the mathematical models presented in Section 2 are simulated considering pure VIV cases and the numerical results are compared with the experimental data presented in Franzini et al. (2012), whose dimensionless parameters are presented in Table 1.

After the numerical–experimental correlation for the pure VIV case, the dynamics of the same cylinder previously simulated is simulated, but now considering the presence of the piezoelectric harvesters on the elastic support. As in Mehmood et al. (2013), the piezoelectric harvesters have capacitance $C_P = 120$ nF, electromechanical coupling term $\theta = 0.00155$ N/V and electric resistance $R = 100\ k\Omega$. Combining these quantities with the cylinder properties presented in Table 1, $\sigma_1 = 0.35$ and $\sigma_2 = 21.4$ are obtained.

Throughout this paper, the dimensionless electric power is discussed in terms of quantities $\bar{\eta}_{el,y}$ or $\bar{\eta}_{el,x}$, corresponding to the time-averaged value during the steady-state response of the dimensionless electric powers. Additionally to the electric power, we also investigate the root-mean square values of the electric tensions ($v_{y,rms}$ and $v_{x,rms}$).

The empirical parameters of the wake-oscillator models are clarified as follows. For the 1-dof VIV, the mentioned parameters are the same suggested by Ogink and Metrikine (2010), assuming $St = 0.1932$ and $C_{D,v} = \overline{C}_D^0 = 1.1856$,

Table 2
Parameters of the wake-oscillator models.

1-dof VIV			2-dof VIV		
ϵ_y	0.05	$U_r < 6.5$	ϵ_y	$0.0045e^{0.228m^*}$	$U_r < 8$
			ϵ_x	0.6	
A_y	4		A_y	2	
			A_x	12	
ϵ_y	0.7	$U_r < 6.5$	ϵ_y	0.7	$U_r > 8$
			ϵ_x	0.7	
A_y	12		A_y	12	
			A_x	12	
$\hat{C}_L^0$	0.3842	$0 < U_r < 15$	$\hat{C}_L^0$	0.3842	$0 < U_r < 15$
$\overline{C_D}^0$	1.1856		$\overline{C_D}^0$	1.1856	
			$\hat{C}_D^0$	0.2	
St	0.1932		St	0.17	

irrespectively of the value of U_r. For the upper-branch response (herein defined in the interval $U_r < 6.5$), ϵ_y and A_y are considered equal to 0.05 and 4 respectively. For the lower-branch response ($U_r > 6.5$), these quantities are $\epsilon_y = 0.7$ and $A_y = 12$.

For the 2-dof VIV wake-oscillator model herein derived and already presented in Section 2.2, the calibration of the parameters is carried out partially based on expressions and values previously presented in the literature. Some parameters are kept invariant with the reduced velocity. The force coefficients are taken as $\hat{C}_L^0 = 0.3842$ and $\overline{C}_D^0 = 1.1856$, the same values suggested by Ogink and Metrikine (2010) for 1-dof VIV. A slightly decrease in the Strouhal number is adopted for the 2-dof VIV case, assuming $St = 0.17$. Notice, however, that this Strouhal number value was already used in the 1-dof VIV context by Grouthier et al. (2014).

The remaining parameters are defined as functions of the reduced velocity. Considering $U_r < 8$, $\epsilon_x = 0.6$ and $\epsilon_y = 0.0045e^{0.228m^*}$ are adopted (see Srinil and Zanganeh, 2012). For this range of reduced velocities, the adoption of $A_y = 2$ and $A_x = 12$ lead to a good correlation with experimental data. The numerical–experimental correlation will be presented in Section 4.1. For $U_r > 8$, we employ $\epsilon_y = \epsilon_x = 0.7$ and $A_x = A_y = 12$. Surprisingly, the calibrated parameters for the 2-dof VIV lower-branch are the same obtained by Ogink and Metrikine (2010) for a 1-dof VIV model. Notice that the calibration approach herein presented focused on a single set of experimental data. The appendix presents some sensitivity studies with respect to the parameters of the 2-dof VIV wake-oscillator model. Investigations focusing on the influence of certain parameters such as the mass ratio parameter are left for a further work. Table 2 presents the parameters of the wake-oscillator models herein adopted.

4. Results and discussions

Subsection 4.1 focuses on the discussion of the pure VIV cases, comparing the numerical results with experimental data. Subsection 4.2 discusses the dynamics of the cylinder subjected to concomitant VIV and piezoelectric effects, highlighting differences between the cases in which the cylinder is free to oscillate in one or in two directions.

4.1. Pure VIV

Fig. 4 presents the numerical–experimental correlation for both 1-dof and 2-dof pure VIV conditions. Discussing the 1-dof VIV case firstly, Fig. 4(a) shows a marked adherence between numerical and experimental data. The maximum oscillation amplitude is $\max\{\hat{y}\} \approx 0.9$, obtained at similar reduced velocities $U_r \approx 6$. Quantitative and qualitative agreements are also found in the range of reduced velocities $7 < U_r < 9.5$, corresponding to the lower branch. Even though the onset of the desynchronization regime occurs for a slightly larger value of reduced velocity in the experimental investigation, the wake-oscillator model can be concluded to represent the experimental data very well.

Next, we analyze the 2-dof VIV condition. Considering both cross-wise and in-line characteristic oscillation curves (Figs. 4(b) and 4(c) respectively), a good adherence with experimental data can be observed. The maximum cross-wise oscillation amplitude from the wake-oscillator model is slightly larger than that experimentally verified. Similarly to what was found for the 1-dof VIV, there is a remarkable adherence of the characteristic oscillation amplitude for the lower branch. The onset of the desynchronization regime occurs at $U_r \approx 10.5$, a value slightly larger than that experimentally observed.

Fig. 4(c) shows the variation of $\hat{x}$ with the reduced velocity. The plot also reveals a marked agreement between numerical and experimental results, including the in-line resonance regime observed in the interval $2 < U_r < 4$. The peak of in-line characteristic oscillation amplitude occurs at $U_r = 6.5$ (numerical results) and $U_r = 6.9$ (experimental data).

The results in this Subsection indicate that the wake-oscillator models used very well reproduce the general aspects of the response of elastically mounted rigid cylinders subjected to 1-dof or 2-dof VIV. The next Subsection discusses the dynamics of the cylinder assembled on an elastic support fitted with piezoelectric harvesters defined by $\sigma_1 = 0.35$ and $\sigma_2 = 21.4$.

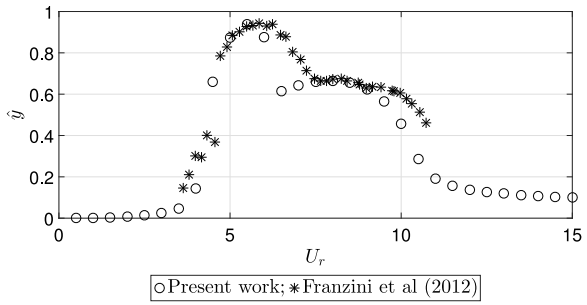

(a) 1-dof VIV.

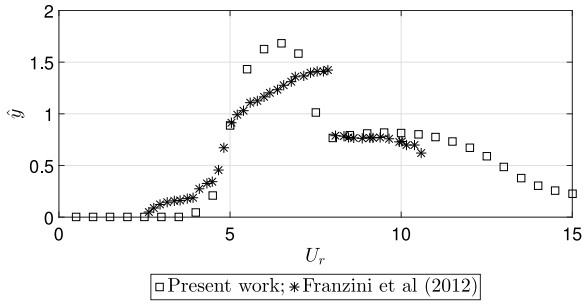

(b) Cross-wise oscillation amplitude: 2-dof VIV.

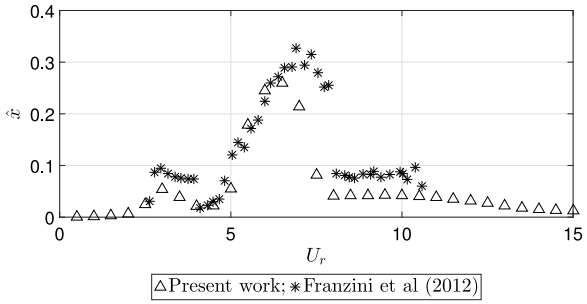

(c) In-line oscillation amplitude: 2-dof VIV.

Fig. 4. Oscillation amplitudes—numerical and experimental results. Pure VIV.

4.2. Concomitant VIV and piezoelectric effects

Fig. 5 shows the characteristic oscillation amplitudes as functions of the reduced velocity. Considering both the 1-dof VIV and the 2-dof VIV cases, the piezoelectric harvester herein adopted does not lead to significant changes in the values of $\hat{x}$ and $\hat{y}$. Unsurprisingly, the piezoelectric harvesters lead to a decrease in the oscillation amplitude when compared to the pure VIV conditions.

Fig. 6 presents examples of displacement time-histories, amplitude spectra and trajectories in the xy plane for both the cases of pure VIV and VIV combined with piezoelectric energy harvesting. In agreement with Fig. 5, the presence of the piezoelectric harvesters with $\sigma_1 = 0.34$ and $\sigma_2 = 21.4$ neither leads to significant decrease in the oscillation amplitude nor to modifications in the narrow-banded character of the amplitude spectra (see Fig. 6(a) to 6(d)).

As well known, the trajectory in the xy plane is governed by both amplitude spectra of the displacement time-histories and the phase-shift between these signals. The marked similarities found in Figs. 6(e) and 6(f) reveal that the piezoelectric effect has practically no influence on the phase-shift between the cross-wise and the in-line displacements.

The variation in the root-mean square (rms) dimensionless electric tension with the reduced velocity is now discussed. Considering the 1-dof VIV condition firstly, Fig. 7 shows that the qualitative aspect of the $v_{y,rms}$ curve follows the one observed for the oscillation amplitude. The maximum value reaches $\max\{v_{y,rms}\} \approx 0.01$ at $U_r = 5.5$. Within interval $6.5 < U_r < 9$, a constant value $v_{y,rms} \approx 0.007$ is obtained.

As aforementioned, electric tension is obtained from both in-line and cross-wise piezoelectric harvesters for the 2-dof VIV. The latter plot reveals that the 2-dof VIV leads a marked enhancement in the values of $v_{y,rms}$ in the range $5 < U_r < 8$.

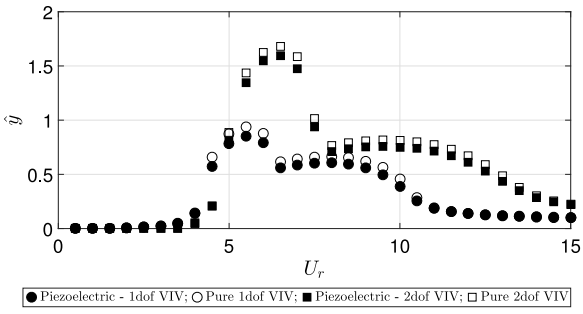

(a) 1-dof VIV.

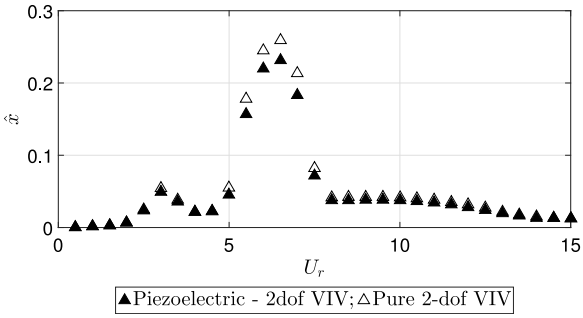

(b) In-line oscillation amplitude: 2-dof VIV.

Fig. 5. Oscillation amplitudes—numerical results. Cylinder assembled to an elastic support with piezoelectric harvesters.

Roughly speaking, the peak of $v_{y,rms}$ is twice that observed for 1-dof VIV and is verified for a slightly larger reduced velocity. Considering the interval $U_r > 8$, the cross-wise electric tension obtained for the 2-dof VIV is larger than that obtained from 1-dof VIV.

Fig. 7 also reveals that the dimensionless electric tension obtained in the in-line harvester is significantly lower than that corresponding to the cross-wise piezoelectric circuit. Notice that $\max\{v_{x,rms}\} \approx \max\{v_{y,rms}\}/4$. Furthermore, electric tension is observed in the in-line harvester only in the range $5 < U_r < 8$.

The dimensionless electric tension time-histories obtained at $U_r = 6$ are presented in Fig. 8. This plot shows a very regular aspect of the time-histories, with a practically constant amplitude. For the 2-dof VIV case, Fig. 8(b) shows that the oscillation frequency of the in-line electric tension is approximately twice that corresponding to the cross-wise one.

In the context of energy harvesting, it is of interest to evaluate the time-averaged electric power at the harvesters. The variation in the energy harvesting efficiency with the reduced velocity is presented in Fig. 9. For the 1-dof VIV case, energy harvesting efficiency reaches its peak $\max\{\bar{\eta}_{el,y}\} \approx 5\%$ at $U_r = 5$. Notice that, despite significant oscillations and electric tension in the interval $7 < U_r < 9$, energy harvesting efficiency is smaller than 1%. In fact, this is not surprising, since Eq. (19) indicates that $\eta_{el,y}$ is proportional to $1/U_r^3$.

The analysis of the same figure reveals interesting features of the 2-dof energy harvesting from VIV. A first aspect that is clearly revealed by this plot is that energy harvesting from in-line oscillations is much less efficient than from cross-wise oscillations.

A second interesting feature can be assessed by comparing the results of $\bar{\eta}_{el,y}$ from 2-dof VIV with those from 1-dof VIV. The maximum energy harvesting efficiency from the 2-dof VIV is $\max\{\bar{\eta}_{el,y}\} \approx 15\%$, practically three times the value obtained for the cylinder free to oscillate only in the cross-wise direction.

In addition to the latter result, the maximum energy harvesting efficiency occurs for a higher reduced velocity in the 2-dof VIV case. This implies an enhancement of the dimensional piezoelectric energy harvesting, as observed in Fig. 10. This plot refers to the electric power that would be harvested from the VIV of a cylinder whose dimensions are presented in Table 1.

A direct comparison of the results from 1-dof or 2-dof VIV indicates that the cylinder free to oscillate in both in-line and in cross-wise direction allows harvesting higher time-averaged electric power $\bar{P}_{el,y}$ for practically the whole range of free-stream velocities herein simulated. Furthermore, the $\max\{\bar{P}_{el,y}\}$ is 2.6 mW for 1-dof VIV and 11 mW for 2-dof VIV.

4.3. A sensitivity study

In this Subsection, we discuss the influence of variations in σ_1 and σ_2 on the harvested power. For this, we consider the particular reduced velocity $U_r = 6$ and a 20×20 grid spanning the intervals $0.07 < \sigma_1 < 1.35$ and $4.28 < \sigma_2 < 107$.

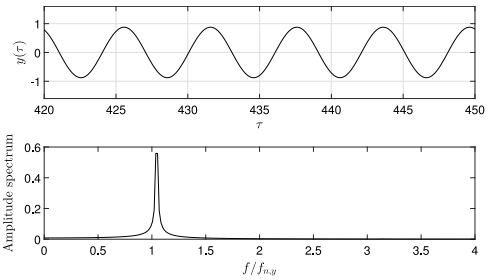

(a) 1-dof pure VIV.

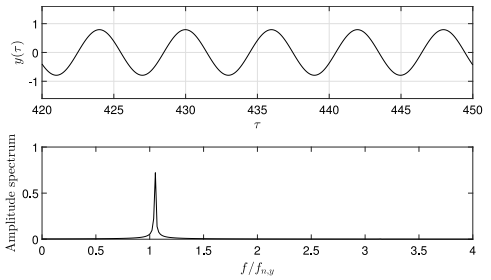

(b) 1-dof pure VIV.

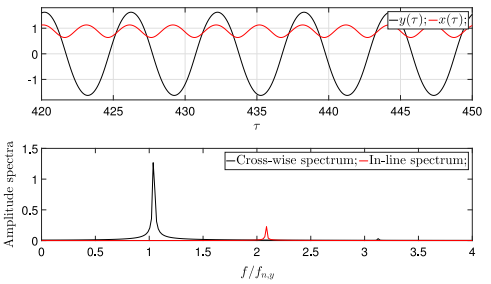

(c) Displacement time-histories and amplitude spectra. Pure VIV.

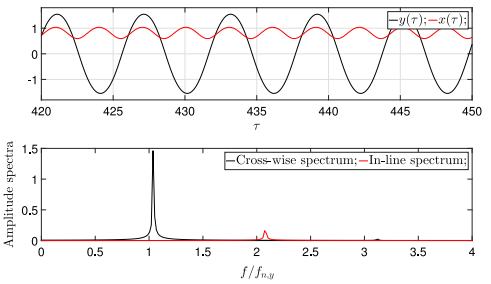

(d) Displacement time-histories and amplitude spectra. $\sigma_1 = 0.34$ and $\sigma_2 = 21.4$.

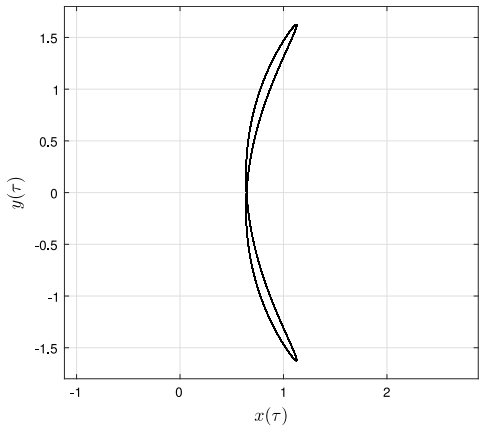

(e) Trajectory in the *xy* plane. Pure VIV.

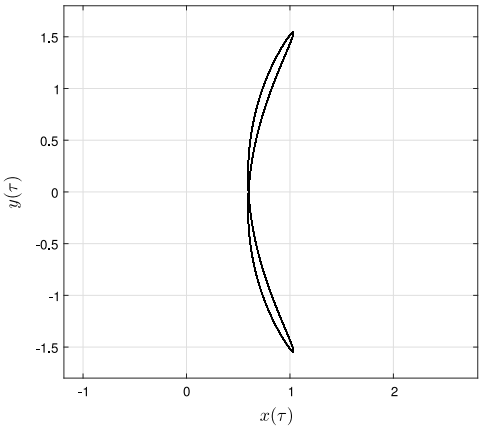

(f) Trajectory in the *xy* plane. $\sigma_1 = 0.34$ and $\sigma_2 = 21.4$.

Fig. 6. Displacement time-histories, amplitude spectra and trajectories in the *xy* plane. $U_r = 6$.

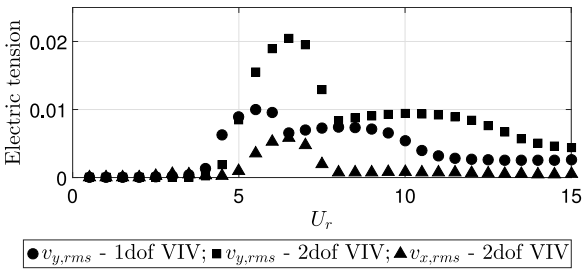

Fig. 7. Dimensionless electric tension (rms) - numerical results. Cylinder assembled to an elastic support with piezoelectric harvesters.

Fig. 11 presents the variation of $\hat{y}$, $\bar{\eta}_{el,y}$ and $\bar{P}_{el,y}$ as functions of σ_1 and σ_2 for both 1-dof and 2-dof VIV conditions. For the sake of better visualization, different scales are adopted.

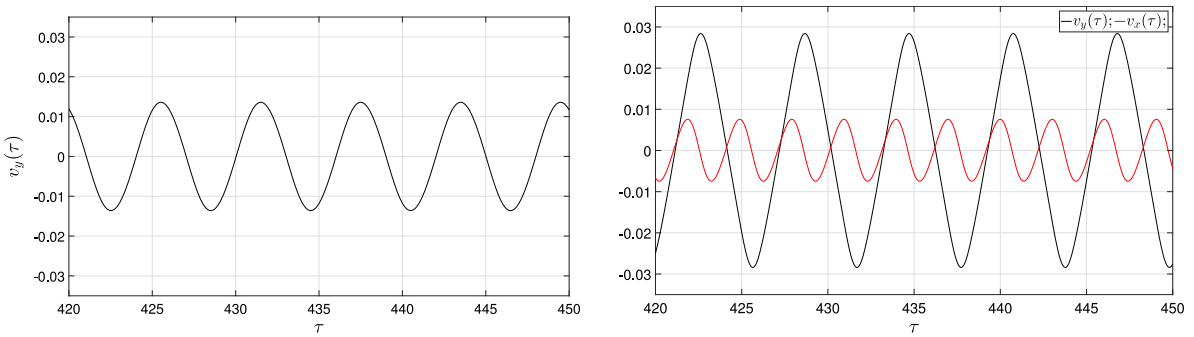

(a) 1-dof VIV. (b) 2-dof VIV.

Fig. 8. Dimensionless electric tension time-histories. $U_r = 6$.

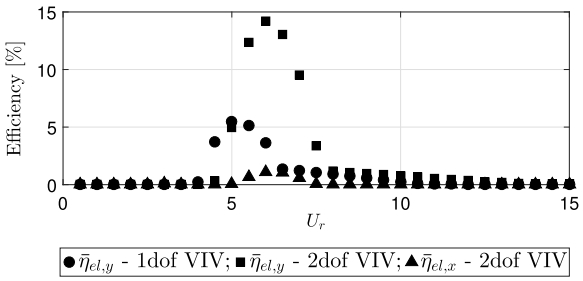

Fig. 9. Energy harvesting efficiency—numerical results. Cylinder assembled to an elastic support with piezoelectric harvesters.

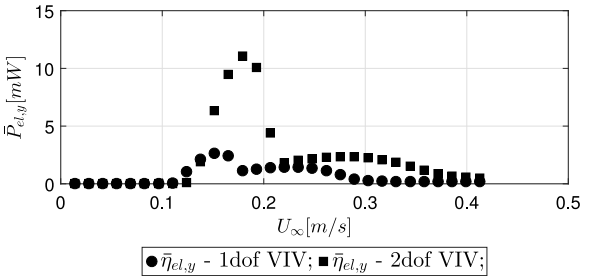

Fig. 10. Time-averaged electric power at the cross-wise harvester—numerical results.

Figs. 11(a) and 11(b) present the variation in cross-wise oscillation amplitude. These plots indicate that significant changes in $\hat{y}$ are observed for $\sigma_2 < 20$ and $\sigma_1 > 0.4$. Notice also that the contour levels follow approximately straight lines.

The analysis of energy harvesting efficiency and electric power harvested are now focused on. Fig. 11(c) to 11(f) show an increase in the values of $\bar{\eta}_{el,y}$ (and, consequently, in the harvested electric power) in the region of σ_1 and σ_2 in which cross-wise oscillation amplitude decreases.

Fig. 9 shows that $\bar{\eta}_{el,y}$ is close to 4% for 1-dof VIV and $\bar{\eta}_{el,y} \approx 15\%$ for 2-dof VIV when $\sigma_1 = 0.35$ and $\sigma_2 = 21.4$ are adopted. Considering $\sigma_2 = 20.5$ (close to the value investigated in Subsection 4.2) and increasing σ_1, Fig. 12 shows that energy harvesting efficiency can reach twice (1-dof VIV) or three times (2-dof VIV) the result presented in the previous Subsection. Furthermore, notice the upward trend of $\bar{\eta}_{el,y}$ for the 2-dof VIV case.

5. Final remarks

The dynamics of a rigid cylinder, mounted onto an elastic support fitted with piezoelectric harvesters and subjected to Vortex-Induced Vibrations (VIV) were numerically investigated. We considered both the cases in which the cylinder is free to oscillate only in the cross-wise direction (1-dof VIV) and in the in-line and in the cross-wise directions concomitantly (2-dof VIV).

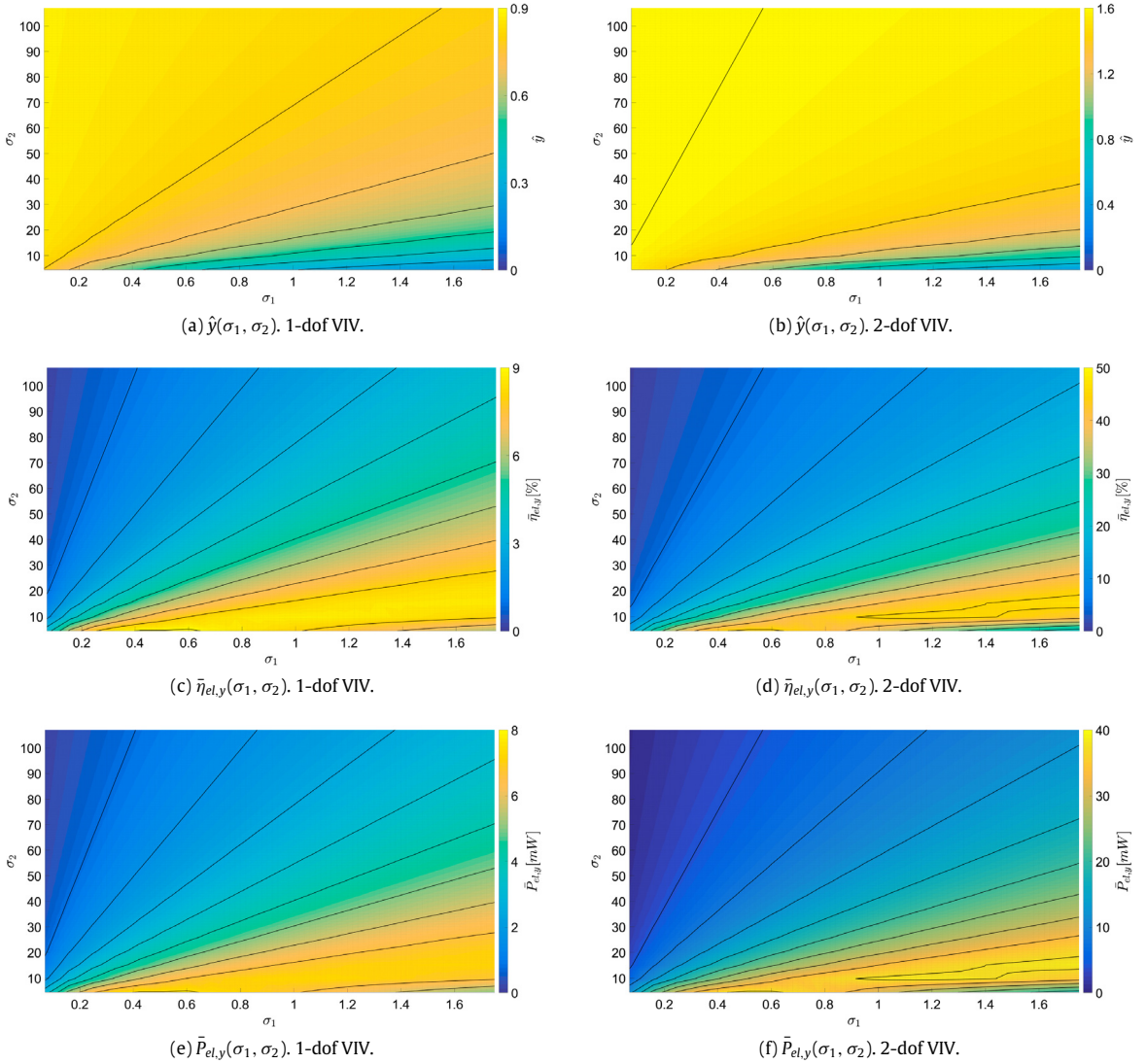

(a) $\hat{y}(\sigma_1, \sigma_2)$. 1-dof VIV.

(b) $\hat{y}(\sigma_1, \sigma_2)$. 2-dof VIV.

(c) $\bar{\eta}_{el,y}(\sigma_1, \sigma_2)$. 1-dof VIV.

(d) $\bar{\eta}_{el,y}(\sigma_1, \sigma_2)$. 2-dof VIV.

(e) $\bar{P}_{el,y}(\sigma_1, \sigma_2)$. 1-dof VIV.

(f) $\bar{P}_{el,y}(\sigma_1, \sigma_2)$. 2-dof VIV.

Fig. 11. Sensitivity study and contour levels. $U_r = 6$.

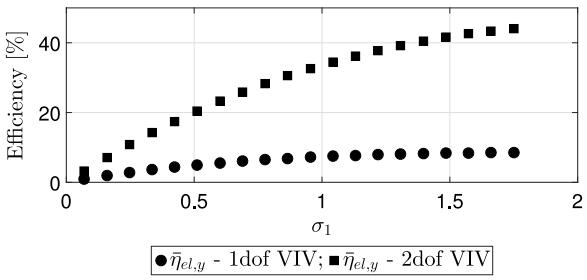

Fig. 12. Variation of $\bar{\eta}_{el,y}$ with σ_1. $U_r = 6$ and $\sigma_2 = 20.5$.

Wake-oscillator models were employed for describing the hydrodynamic loads. For the 1-dof VIV, a nonlinear wake oscillator model previously published was adopted. A fully nonlinear wake oscillator model was derived for the 2-dof VIV condition. Linear constitutive equations were used aiming at modeling the piezoelectric harvesters. The mathematical

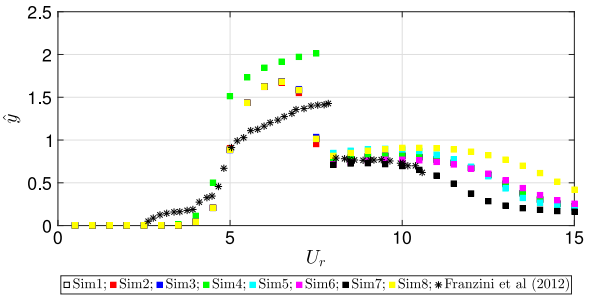

(a) Cross-wise direction.

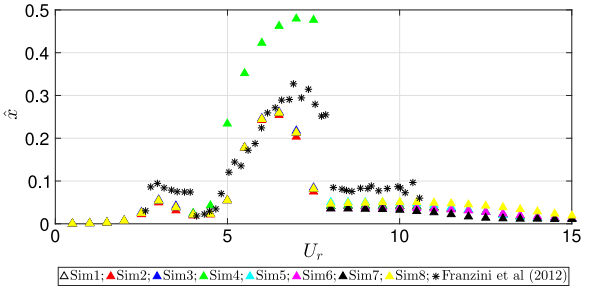

(b) In-line direction.

Fig. A.13. Example of sensitivity study with respect to some parameters of the wake-oscillator model. Pure 2-dof VIV.

models were obtained and numerically integrated, allowing obtaining curves of oscillation amplitude, electric tension and time-averaged electric power as functions of the reduced velocity.

Special focus was placed on the comparison between the results from 1-dof and 2-dof VIV for a particular set of dimensionless parameters that govern the solid–fluid-electric systems. To the authors knowledge, energy harvesting from 2-dof VIV is not commonly found in the literature.

As the major contribution of this paper, we highlight the marked increase in the energy harvesting efficiency from 2-dof VIV when compared to that obtained from 1-dof VIV considering the same parameters of the piezoelectric harvesters. The maximum energy harvesting efficiency was shown to drop from $\bar{\eta}_{el,y} \approx 5\%$ to $\bar{\eta}_{el,y} \approx 15\%$ when 2-dof VIV is considered instead of only cross-wise displacements.

Additionally to the comparison between the dynamics of the cylinder with one and two degrees of freedom, a sensitivity study was conducted with respect to the influence of the dimensionless quantities that define the piezoelectric harvesters. Considering reduced velocity $U_r = 6$, this sensitivity study showed that the energy harvesting efficiency should be significantly increased.

Further works include extending the sensitivity studies, considering other reduced velocities and modifications in the structural dimensionless quantities, particularly the influence of the in-line to cross-wise natural frequencies ratio.

Acknowledgments

The first author is grateful to the Brazilian National Council for Research (CNPq) for the grant 310595/2015-0. The second author acknowledges the São Paulo Research Foundation (FAPESP) for his undergraduate scholarship, grant 2014/19530-2. This work is part of a research project on renewable energy from oceans supported by NAP-OS (University of São Paulo Nucleus for Research Support—Sustainable Ocean). Finally, the authors acknowledge Prof. Celso Pesce, from Escola Politécnica, University of São Paulo, for his valuable comments.

Appendix. A study on the sensitivity of the parameters of the 2-dof VIV wake-oscillator model

This Appendix presents a sensitivity study into the response of 2-dof VIV wake-oscillator model with respect to parameters A_x, A_y, ϵ_x and ϵ_y. For this, eight pure 2-dof VIV simulations are carried out according to the nomenclature presented in Table A.3, being Sim1 the case discussed in Subsection 4.1. The remaining parameters of the wake-oscillator models are those already presented in Subsection 4.1.

Fig. A.13 presents the oscillation amplitudes obtained from the simulations defined in Table A.3. Firstly, we discuss the results related to variations in the parameters adopted for $U_r < 8$. The first study involves Sim2, Sim3 and Sim4. As verified

Table A.3
Parameters of the wake-oscillator models—sensitivity study.

Simulation	$U_r < 8$		$U_r > 8$			
	A_x	A_y	ϵ_x	ϵ_y	A_x	A_y
Sim1	12	2	0.7	0.7	12	12
Sim2	8	2	0.7	0.7	12	12
Sim3	14	2	0.7	0.7	12	12
Sim4	12	4	0.7	0.7	12	12
Sim5	12	2	0.5	0.5	12	12
Sim6	12	2	0.9	0.9	12	12
Sim7	12	2	0.7	0.7	10	10
Sim8	12	2	0.7	0.7	14	14

in Fig. A.13, there is a very good agreement in the results from Sim2 and Sim3. Hence, small variations around $A_x = 12$ do not lead to significant changes in the oscillation amplitudes. On the other hand, increasing A_y to 4 implies a significant increase in both cross-wise (Fig. A.13(a)) and in-line (Fig. A.13(b)) oscillation amplitudes.

Now, focus is placed on the influence of variations in the parameters for $U_r > 8$, corresponding to simulations Sim5, Sim6, Sim7 and Sim8. Notice that, in this interval, both parameters ϵ_x and ϵ_y are different from the values suggested by Srinil and Zanganeh (2012). Figs. A.13(a) and A.13(b) reveal that only Sim8 presents oscillation amplitudes significantly different from the other simulations. This result indicates that the oscillation amplitude are less sensitive to variations in ϵ_x and ϵ_y (Sim5 and Sim6) around $\epsilon_x = \epsilon_y = 0.7$. Yet, the increase in $A_x = A_y$ to 14 (Sim8) leads to larger oscillation amplitudes observed in this range of reduced velocities.

Note that the sensitivity study presented in this Appendix focuses on the variations of some parameters of the wake-oscillator model around the values defined in Subsection 3. A comprehensive calibration of these parameters must include other physical parameters of the system such as the mass ratio parameter m^*. This is left for further work.

References

Akaydin, H.D., Elvin, N., Andreopoulos, 2012. The performance of a self-excited fluidic energy harvester. Smart Mater. Struct. 21, 1–13. http://dx.doi.org/10.1088/0964-1726/21/2/025007.

Antoine, G.O., de Langre, E., Michelin, S., 2016a. Optimal energy harvesting from vortex-induced vibrations of cables. http://dx.doi.org/10.1098/rspa.2016.0583.

Antoine, G.O., Michelin, S., de Langre, E., 2016b. Optimal energy harvesting from vortex-induced vibrations of cables. In: Proceedings of the ASME 2016 International Conference on Ocean, Offshore and Arctic Engineering - OMAE2016.

Arionfard, H., Nishi, Y., 2017. Experimental investigation of a drag assisted vortex-induced vibration energy converter. J. Fluids Struct. 68, 48–57. http://dx.doi.org/10.1016/j.jfluidstructs.2016.10.002.

Barrero-Gil, A., Alonso, G., Sanz-Andres, A., 2010. Energy harvesting from transverse galloping. J. Sound Vib. 329, 2873–2883. http://dx.doi.org/10.1016/j.jsv.2010.01.028.

Bearman, P.W., 1984. Vortex shedding from oscillating bluff bodies. Annu. Rev. Fluid Mech. 16, 195–222.

Bearman, P.W., 2011. Circular cylinders wake and vortex-induced vibrations. J. Fluids Struct. 27, 648–658. http://dx.doi.org/10.1016/j.jfluidstructs.2011.03.021.

Bernitsas, M.M., Raghavan, K., Ben-Simos, Y., Garcia, E.M.H., 2006. VIVACE (Vortex Induced Vibration Aquatic Clean Energy): A new concept in generation of clean and renewable energy from fluid flow. In: Proceedings of OMAE2006 - International Conference on Offshore Mechanics and Artic Engineering.

Blevins, R., 2001. Flow-Induced Vibration. Krieger.

Blevins, R.D., Coughran, C.S., 2009. Experimental investigation of vortex-induced vibration in one and two dimensions with variable mass, damping, and Reynolds number. J. Fluids Eng. 131, 101202–1 –101202–7. http://dx.doi.org/10.1115/1.3222904.

Bunzel, L.O., Franzini, G.R., 2017. Numerical studies on piezoelectric energy harvesting from vortex-induced vibrations considering cross-wise and in-line oscillations. In: Proceedings of the 9th European Nonlinear Dynamics Conference - ENOC2017.

Chaplin, J.R., Bearman, P.W., Cheng, Y., Fontaine, E., Graham, J.M.R., Herfjord, K., Huer Huarte, F.J., Isherwood, M., Lambracos, K., Larsen, C.M., Meneghini, J.R., Moe, G., Pattenden, R., Triantafyllou, M.S., Willden, R.H.J., 2005a. Blind predictions of laboratory measurements of vortex-induced vibrations of a tension riser. J. Fluids Struct. 21, 25–40.

Chaplin, J.R., Bearman, P.W., Huer Huarte, F.J., Pattenden, R.J., 2005b. Laboratory measurements of vortex-induced vibrations of a vertical tension riser in a stepped current. J. Fluids Struct. 21, 3–24.

Dai, H.L., Abdelkefi, A., Wang, L., 2014. Piezoelectric energy harvesting from concurrent vortex-induced vibrations and base excitation. Nonlinear Dynam. 77, 967–981. http://dx.doi.org/10.1007/s11071-014-1355-8.

Dhanwani, M.A., Sarkar, A., Patnaik, B.S.V., 2013. Lumped parameter models of vortex-induced vibration with application to the design of aquatic energy harvester. J. Fluids Struct. 43, 302–324. http://dx.doi.org/10.1016/j.jfluidstructs.2013.09.008.

Doaré, O., Michelin, S., 2011. Piezoelectric coupling in energy harvesting fluttering flexible plates: Linear stability analysis and conversion efficiency. J. Fluids Struct. 27, 1357–1375. http://dx.doi.org/10.1016/j.jfluidstructs.2011.04.008.

Erturk, A., Inman, D.J., 2011. Piezoeletric Energy Harvesting. John Wiley & Sons.

Facchinetti, M.L., de Langre, E., Biolley, F., 2004. Coupling of structure and wake oscillators in vortex-induced vibrations. J. Fluids Struct. 19, 123–140. http://dx.doi.org/10.1016/j.jfluidstructs.2003.12.004.

Fernandes, A.C., Armandei, M., 2014. Low-head hydropower extraction based on torsional galloping. Renew. Energy 69, 447–452. http://dx.doi.org/10.1016/j.renene.2014.03.057.

Franzini, G.R., Gonçalves, R.T., Meneghini, J.R., Fujarra, A.L.C., 2013. One and two degrees-of-freedom vortex-induced vibration experiments with yawed cylinders. J. Fluids Struct. 42, 401–420. http://dx.doi.org/10.1016/j.jfluidstructs.2013.07.006.

Franzini, G.R., Gonçalves, R.T., Meneghini, J.R., Fujarra, A.L.C., 2012. Comparison between force measurements of one and two degrees-of-freedom VIV on cylinder with small and large mass ratio. In: Proceedings of the 10th FIV 2012 - International Conference on Flow-Induced Vibrations Conference (& Flow-Induced Noise).
Franzini, G.R., Santos, R.C.S., Pesce, C.P., 2016. Energy harvesting from transverse galloping enhanced by parametric excitation. In: Proceedings of the 11th International Conference on Flow-Induced Vibration - FIV2016.
Franzini, G.R., Santos, R.C.S., Pesce, C., 2017. A numerical study on piezoelectric energy harvesting by combining transverse galloping and parametric instability phenomena. J. Mar. Sci. Appl. http://dx.doi.org/10.1007/s11804-017-1439-1. online.
Freire, C.M., Meneghini, J.R., 2010. Experimental investigation of VIV on a circular cylinder mounted on an articulated elastic base with two degrees-of-freedom. In: IUTAM Symposium on Bluff Bodies Wakes and Vortex-Induced Vibrations - BBVIV6.
Fujarra, A., Pesce, C., Flemming, F., Williamson, C., 2001. Vortex-induced vibration of a flexible cantilever. J. Fluids Struct. 15, 651–658.
Furnes, G.K., Sørensen, 2007. Flow induced vibrations mmodele by coupled non-linear oscillators. In: Proceedings of the Seventeenth (2007) International Offshore and Polar Engineering Conference - ISOPE 2007.
Gabbai, R., Benaroya, H., 2005. An overview of modeling and experiments of vortex-induced vibration of circular cylinders. J. Sound Vib. 282, 575–616. http://dx.doi.org/10.1016/j.jsv.2004.04.017.
Gabbai, R., Benaroya, H., 2008. A first-principles derivation procedure for wake-body models in vortex-induced vibration: Proof-of-concept. J. Sound Vib. 312, 19–38. http://dx.doi.org/10.1016/j.jsv.2007.07.086.
Grouthier, C., Michelin, S., Bourguet, R., Modarres-Sadeghi, Y., de Langre, E., 2014. On the efficiency of energy harvesting using vortex-induced vibrations of cables. J. Fluids Struct. 49, 427–440. http://dx.doi.org/10.1016/j.jfluidstructs.2014.05.004.
Grouthier, C., Michelin, S., de Langre, E., 2012. Optimal energy harvesting by vortex-induced vibrations in cables. In: Proceedings of the 10th FIV 2012 - International Conference on Flow-Induced Vibrations Conference (& Flow-Induced Noise).
Hartlen, R.T., Currie, T.G., 1970. Lift-oscillator model of vortex-induced vibration. J. Eng. Mech. Div. EM5, 577–591.
Hémon, P., Amandolese, X., Andrianne, T., 2017. Energy harvesting from galloping of prisms: A wind tunnel experiment. J. Fluids Struct. 70, 390–402. http://dx.doi.org/10.1016/j.jfluidstructs.2017.02.006.
Hover, F.S., Miller, S.N., Triantafyllou, M.S., 1997. Vortex-induced vibration of marine cables: Experiments using force feedback. J. Fluids Struct. 11, 307–326.
Huera-Huarte, F.J., Bearman, P.W., 2009a. Wake structures and vortex-induced vibrations of a long flexible cylinder - part 1: Dynamic response. J. Fluids Struct. 25, 969–990.
Huera-Huarte, F.J., Bearman, P.W., 2009b. Wake structures and vortex-induced vibrations of a long flexible cylinder - part 2: Drag coefficients and vortex modes. J. Fluids Struct. 25, 991–1006.
Iwan, W.D., Blevins, R.D., 1974. A model for vortex-induced oscillation of structures. J. Appl. Mech. 41, 581–586.
Jauvtis, N., Williamson, C.H.K., 2004. The effect of two degrees of freedom on vortex-induced vibration at low mass and damping. J. Fluid Mech. 509, 23–62. http://dx.doi.org/10.1017/S0022112004008778.
Khalak, A., Williamson, C.H.K., 1999. Motions, forces and modes transitions in vortex-induced vibration at low Reynolds number. J. Fluids Struct. 13, 813–851. http://dx.doi.org/10.1006/jfls.1999.0236.
Lyons, G.J., Patel, M.H., 1986. A prediction techinique for vortex induced transverse response of marine risers and tethers. J. Sound Vib. 111, 467–487.
Mehmood, A., Abdelkefi, A., Hajj, A.A., Nayfeh, A.H., Akthar, I., Nuhait, A.O., 2013. Piezoelectric energy harvesting from vortex-induced vibrations of circular cylinder. J. Sound Vib. 332, 4656–4667. http://dx.doi.org/10.1016/j.jsv.2013.03.033.
Naudascher, E., Rockwell, D., 2005. Flow-Induced Vibrations - an Engineering Guide. Dover.
Nishi, Y., Fukuda, K., Shinohara, W., 2017. Experiemental energy harvesting from fluid flow by using two vibrating masses. J. Sound Vib.http://dx.doi.org/10.1016/j.jsv.2017.01.037.
Ogink, R.H.M., Metrikine, A.V., 2010. A wake oscillator with frequency dependent coupling for the modeling of vortex-induced vibration. J. Sound Vib. 329, 5452–5473. http://dx.doi.org/10.1016/j.jsv.2010.07.008.
Parkinson, G., 1989. Phenomena and modelling of flow-induced vibration of bluff bodies. Prog. Aerosp. Sci. 26, 169–224.
Païdoussis, M.P., Price, S.J., de Langre, E., 2011. Fluid-Structure Interactions - Cross-Flow-Induced Instabilities. Cambridge University Press.
Pesce, C.P., Fujarra, A.L.C., 2000. Vortex-induced vibrations and jump phenomenon: Experiments with a clamped flexible cylinder in water. Int. J. Offshore Polar Eng. 10, 26–33.
Sarpkaya, T., 1977. In-line and transverse forces on cylinders in oscillatory flow at high Reynolds numbers. J. Ship Res. 21.
Sarpkaya, T., 1979. Vortex-induced oscillations. J. Appl. Mech. 46, 241–258.
Sarpkaya, T., 1986. Force on a circular cylinder in viscous oscillatory flow at low Keulegan-Carpenter numbers. J. Fluid Mech. 165, 61–71. http://dx.doi.org/10.1017/S0022112086002999.
Sarpkaya, T., 2004. A critical review of the intrinsic nature of vortex-induced vibrations. J. Fluids Struct. 19, 389–447. http://dx.doi.org/10.1016/j.jfluidstructs.2004.02.005.
Skop, R.A., Balasubramanian, S., 1997. A new twist on an old model fo vortex-induced excitations. J. Fluids Struct. 11, 395–412.
Skop, R.A., Griffin, O.M., 1975. On a theory for the vortex-excited oscillations of flexible cylindrical structures. J. Sound Vib. 41, 263–274.
Soti, A.K., Thompson, M.C., Sheridan, J., Bhardwaj, R., 2017. Harnessing electrical power from vortex-induced vibrations of a circular cylinder. J. Fluids Struct. 70, 360–373. http://dx.doi.org/10.1016/j.jfluidstructs.2017.02.009.
Srinil, N., Zanganeh, H., 2012. Modelling of coupled cross-flow/in-line vortex-induced vibrations using double Duffing and van der Pol oscillators. Ocean Eng. 53, 83–97. http://dx.doi.org/10.1016/j.oceaneng.2012.06.025.
Stappenbelt, B., Lalji, F., 2008. Vortex-induced vibration super-upper branch boundaries. Int. J. Offshore Polar Eng. 18, 99–105.
Sumer, B.M., Fredsøe, J., 1988. Transverse vibrations of an elastically mounted cylinder exposed to an oscillating flow. J. Offshore Mech. Arctic Eng. 110, 387–394.
Tang, L., Païdoussis, M.P., Jiang, J., 2009. Cantilever flexible plates in axial flow: Energy transfer and the concept of flutter-mill. J. Sound Vib. 326, 263–276. http://dx.doi.org/10.1016/j.jsv.2009.04.041.
Williamson, C.H.K., 1996. Vortex dynamics in the cylinder wake. Annu. Rev. Fluid Mech. 28, 477–539.
Williamson, C.H.K., Govardhan, R.N., 2004. Vortex-induced vibrations. Annu. Rev. Fluid Mech. 36, 413–455. http://dx.doi.org/10.1146/annurev.fluid.36.050802.122128.
Williamson, C.H.K., Roshko, A., 1988. Vortex formation in the wake of an oscillating cylinder. J. Fluids Struct. 2, 355–381.
Xiao, Q., Zhu, Q., 2014. A review on flow energy harversters based in flapping foils. J. Fluids Struct. 46, 174–191. http://dx.doi.org/10.1016/j.jfluidstructs.2014.01.002.
Zanganeh, H., Srinil, N., 2014. Characterization of variable hydrodynamic coefficients and maximum responses in two-dimensional vortex-induced vibrations with dual resonances. J. Vib. Acoust. 136, 051014–1 –051014–15. http://dx.doi.org/10.1115/1.4027805.
Zhang, L., Abdelkefi, A., Dai, H.L., Naseer, R., Wang, L., 2017. Design and experimental analysis of broadband energy harvesting from vortex-induced vibrations. J. Sound Vib. 408, 210–219. http://dx.doi.org/10.1016/j.jsv.2017.07.029.